coatings

MDPI

Article

The Effect of Charged Ag Nanoparticles on Thin Film Growth during DC Magnetron Sputtering

Gil-Su Jang, Du-Yun Kim and Nong-Moon Hwang *

Department of Material Science and Engineering, College of Engineering at Seoul National University, 1 Gwanak-ro, Gwanak-gu, Seoul 08826, Korea; gsjang@snu.ac.kr (G.-S.J.); kdy9271@snu.ac.kr (D.-Y.K.)
* Correspondence: nmhwang@snu.ac.kr; Tel.: +82-2-880-8922

Received: 6 July 2020; Accepted: 24 July 2020; Published: 28 July 2020

Abstract: The possibility that charged nanoparticles (CNPs) are generated in the gas phase during direct current (DC) magnetron sputtering of Ag is studied. Sputtered Ag particles could be captured on an ultrathin amorphous carbon membrane for transmission electron microscopy (TEM) observation. It is confirmed that the average particle size and the total area of deposition under the condition of the positive bias applied to the substrate are bigger than those under the condition of the negative bias applied to the substrate. The results indicate that some of the sputtered Ag particles are negatively charged. To evaluate the contribution of negatively-charged particles to the film growth, Ag thin films were deposited for 30 min on the Si substrate with the substrate biases of −300, 0 and +300 V and analyzed by field-emission scanning electron microscopy (FESEM), X-ray diffraction (XRD) and four-point probe. When +300 V was applied to the substrate, the film growth rate was highest with the film thickness of 85.0 nm, the crystallinity was best with the smallest full width at half maximum (FWHM) value of 0.44 and the resistivity was smallest with 3.67 μΩ·cm. In contrast, when −300 V was applied to the substrate, the film growth rate was lowest with the film thickness of 68.9 nm, the crystallinity was worst with the largest FWHM value of 0.53 and the resistivity was largest with 8.87 μΩ·cm. This result indicates that the charge plays an important role in film growth and can be a new process parameter in sputtering.

Keywords: charged particle; thin films; DC sputtering; Ag; substrate bias

1. Introduction

Ag thin films and nanoparticles are used in optical applications [1–5], microelectronics [6,7] and biomedical applications [8–10] because of their excellent electrical and optical properties, good chemical and thermal stability and antibacterial effects. Ag thin films and nanoparticles are made in various ways, such as thermal evaporation [3,11], direct current (DC) sputtering [12,13], radio frequency (RF) sputtering [14–16] and high power impulse magnetron sputtering (HiPIMS) [17,18].

In general, the thin film deposition mechanism is described as a terrace–ledge–kink (TLK) model [19], where an adatom moves around on the terrace until it finds a kink at the ledge; it is then incorporated into a crystal. In this model, the building block is an individual atom, molecule or ion. This way of crystal growth is called classical crystallization. However, some deposition behavior of thin films that is difficult to explain by the conventional TLK model has been observed. Such deposition behavior could be successfully explained by the new film growth mechanism, where the building block is nanoparticles generated in the gas phase. This new mechanism is called non-classical crystallization [20–26].

Hwang et al. [26] extensively studied the thin film growth by non-classical crystallization in a chemical vapor deposition (CVD) process. They suggested that during the CVD process, electrically charged nanoparticles (CNPs) are formed in the gas phase, and these CNPs can be a major deposition flux of thin

films. In this case, the deposition unit of thin films is neither an atom nor molecule but a nanoparticle. Additionally, here, an electric charge carried by nanoparticles plays an important role in the evolution of dense films by non-classical crystallization. They called this new thin film growth mechanism "the theory of charged nanoparticles (TCN)." According to the TCN, if the nanoparticles are neutral, a porous thin film tends to be formed by random Brownian coagulation, but if they are charged, a dense thin film tends to be formed in a highly orderly manner of deposition by self-assembly. Besides, when the particles become charged, the binding force between atoms weakens, so the particles have a high atomic mobility. As a result, CNPs undergo liquid-like coalescence when they land on the growing surface, and because of such liquid-like coalescence, even epitaxial films can be grown by CNPs. For example, a fully epitaxial silicon film could be grown on a silicon wafer at 550 °C under the bias of −1000 V during radio frequency plasma-enhanced chemical vapor deposition (RF-PECVD) [27].

In relation to the weakening of the binding force between atoms in CNPs, Clare et al. [28] reported by ab initio calculations that the bond strengths of Si–Si and Si–H are weakened by the presence of positive or negative charges in silane (SiH_4) and disilane (Si_2H_6) molecules.

Although the film growth by CNPs has been studied extensively in CVD, not much work has been done in physical vapor deposition (PVD). Jeon et al. [11] confirmed the generation of charged Ag nanoparticles during thermal evaporation by current measurements combined with the bias experiment. Kwon et al. [29] confirmed the generation of charged Ti nanoparticles and their contribution to film growth during RF magnetron sputtering. This means that it is highly probable that CNPs would also be generated in the DC magnetron sputtering.

The purpose of this study was to confirm the generation of CNPs and their contribution to film growth during DC magnetron sputtering of Ag. For this, we tried to capture nanoparticles on a membrane for transmission electron microscopy (TEM) and to deposit films under the bias applied to the substrate holder.

2. Materials and Methods

Figure 1a shows a schematic of the DC magnetron sputtering system. An Ag target 7.62 cm in diameter was used. The distance between the Ag target and substrate was 24 cm. The reason why this distance was made larger than that typically used in sputtering was to examine the effect of the electric bias applied to the substrate holder. An ultrathin amorphous carbon TEM membrane (Ted Pella, Inc., Redding, CA, USA) for capturing sputtered particles was placed on a substrate holder, which was electrically insulated from the grounded sputter system in order to apply the electric bias. By particle capturing, we mean the deposition of the sputtering flux on the TEM membrane for a short exposure time, usually less than 10 s. A p-type Si (100) substrate was used for film deposition. The Cu mesh, which was grounded, was installed above the substrate holder to minimize the effect of the substrate bias on the plasma. The hole size of the grounded mesh was 150 μm, which was determined not to exceed the Debye length of the plasma [30].

A shutter was placed above the grounded mesh to control the particle capturing or film deposition. By opening or closing the shutter, the time for capturing and deposition could be controlled. The current of the substrate holder was measured during the sputtering process in order to check whether any of the sputtering flux was charged. The current was measured by a pico-ammeter (KEITHLEY 6487, Tektronix, Cleveland, OH, USA). Figure 1b shows the current measured on the substrate holder during the time interval when the plasma for sputtering was turned on and off. Note that no bias was applied to the substrate holder. Definitely, an appreciable amount of negative current was measured as soon as the plasma was turned on. Most of the flux carrying a negative charge would be electrons. However, we cannot rule out the possibility that some of the sputtered flux might carry the negative charge. This possibility can be confirmed by the bias experiment.

DC plasma power, Ar gas pressure and substrate temperature were 200 W, 1.33 Pa (10 mTorr) and room temperature, respectively, for all experiments. To confirm that the charged flux contributes to the

deposition, the capturing and deposition behavior were compared for the samples prepared under the biases of +300, 0, and −300 V applied to the substrate holder.

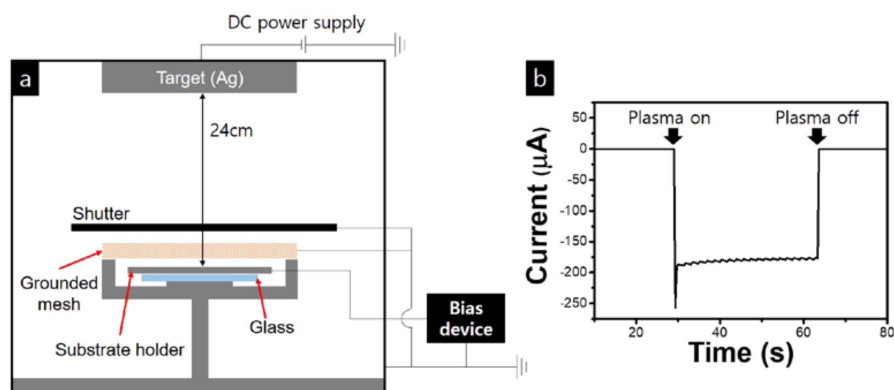

Figure 1. (**a**) Schematic of the DC sputtering system and (**b**) the current measured on the substrate holder at the plasma power of 200 W.

The bias applied to the substrate affects the plasma. To eliminate this effect, a grounded mesh was installed between the plasma and the substrate. As the bias applied to the substrate increases, the Debye length of the plasma decreases. In order for the bias not to affect the plasma, the hole size of a grounded mesh should be smaller than the Debye length. If the hole size is too small, the sputtered flux coming to the substrate would become very small and the experiment would not be appropriate. If the bias is too small, the substrate bias becomes smaller than the kinetic energy of the sputtered particles, so the bias would not have any effect. Considering these two factors, the biases of ±300 V were chosen.

To see the time evolution of particles, the capturing experiments were performed for 1, 3, 5, 7 and 10 s under all bias conditions. Additionally, in order to study the effects of the charged flux on the film properties, the thin film was deposited for 30 min under the three bias conditions mentioned above.

The Ag particles captured on the amorphous carbon membrane were observed by TEM (FEI, Tecnai F20, Hillsboro, OR, USA). The open source software ImageJ (1.51k, National Institutes of Health, Bethesda, MD, USA) was used to analyze the TEM images. ImageJ analyzed the images in pixels. It calculated the particle size, the nanoparticle density and the total area by setting the appropriate threshold value. The microstructure of the Ag films was investigated by field-emission scanning electron microscopy (FESEM, Carl Zeiss, SUPRA, Oberkochen, Germany). TEM and FESEM were operated at accelerating voltages of 200 and 2 kV, respectively. The crystallinity of the films was analyzed by X-ray diffraction (XRD, PANalytical, X'pert-Pro, Almelo, The Netherlands) at a 2θ scanning range of 30°–80° with the Cu Kα (λ = 1.5418 Å) source. The resistivity of Ag films was measured using a four-point probe (CMT-SR2000N, Materials Development Corporation, Founex, Switzerland).

3. Results and Discussion

3.1. Capturing CNPs during DC Sputtering with an Ag Target

Figure 2 shows the time evolution of TEM images of sputtered Ag particles captured on the ultrathin amorphous carbon membrane under the substrate bias of 0 V or in the absence of the bias. Ag particles captured for 1, 3, 5, 7 and 10 s had the average diameters of 1.7 ± 0.06, 2.0 ± 0.05, 2.2 ± 0.14, 2.6 ± 0.09 and 3.1 ± 0.08 nm; and the nanoparticle densities of 18,415 ± 421, 24,068 ± 418, 28,281 ± 930, 28,606 ± 531 and 22,736 ± 269 per μm^2, respectively. Those data were estimated using an image analysis tool of ImageJ (1.51k) [31]. The size of Ag particles continued to increase with the capture time. However, the number density increased up to 7 s and then decreased at 10 s.

Most of Ag particles captured for 1 s in Figure 2a were not crystalline but amorphous. This aspect was revealed by the high resolution TEM (HRTEM) image and the fast Fourier-transform (FFT) inset

in Figure 3a. As the size of Ag particles increases, they tend to be crystalline. This transition from amorphous to crystalline phase occurred at ~2.5 nm, where roughly 50% of them were amorphous and the other 50% were crystalline. Most of Ag particles captured for 10 s in Figure 2e, which had the average size of ~3.1 nm, were crystalline, as revealed by the high resolution TEM image and the FFT inset in Figure 3b.

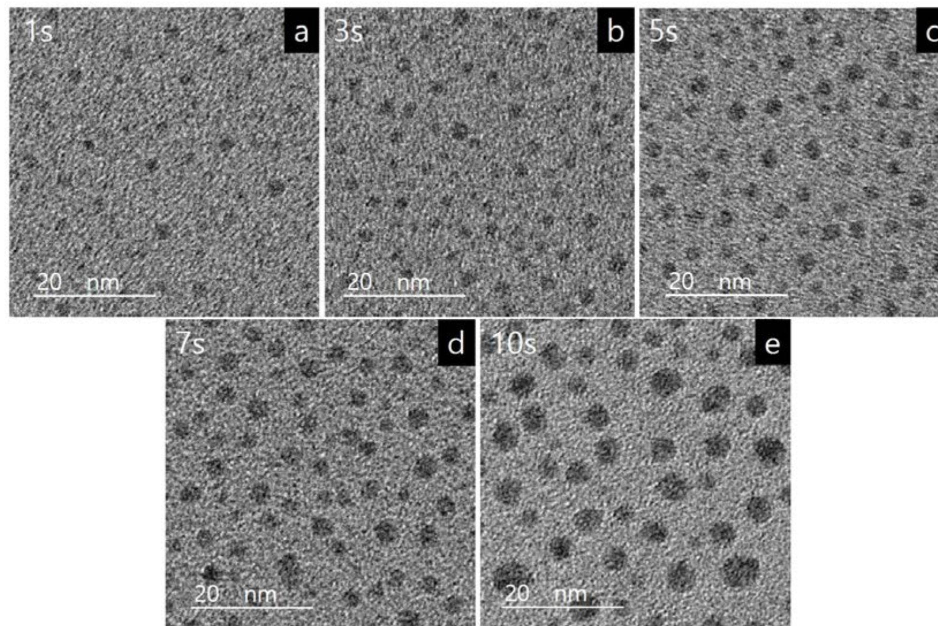

Figure 2. TEM images of Ag particles captured on an amorphous carbon membrane at the substrate bias of 0 V for (**a**) 1 s, (**b**) 3 s, (**c**) 5 s, (**d**) 7 s and (**e**) 10 s.

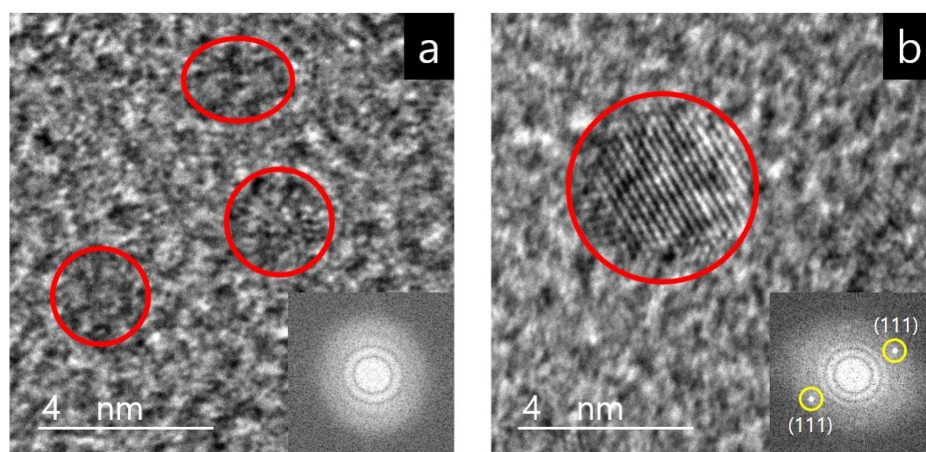

Figure 3. HRTEM image and FFT information (inset of the lower right in the image) of Ag sputtered particles captured on an amorphous carbon membrane at the substrate bias of 0 V for (**a**) 1 s and (**b**) 10 s.

Figure 4 shows the time evolution of TEM images of the sputtered Ag particles captured on the amorphous carbon membrane under the substrate bias of +300 V. Ag particles captured for 1, 3, 5, 7 and 10 s had the average diameters of 1.7 ± 0.12, 2.0 ± 0.1, 2.3 ± 0.09, 3.0 ± 0.22 and 3.4 ± 0.14 nm; and the nanoparticle densities of 18,911 ± 731, 31,549 ± 1076, 30,635 ± 647, 23,681 ± 585 and 20,289 ± 487 per μm^2, respectively. Although the average size of Ag particles continued to increase with the capture time, the number density increased up to 3 s and then decreased up to 10 s.

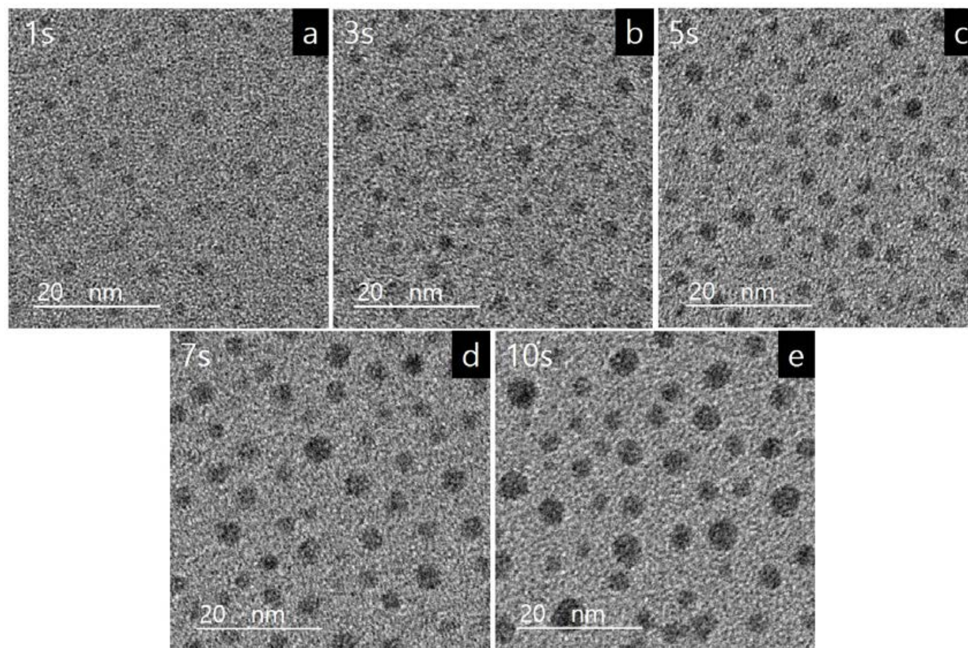

Figure 4. TEM images of Ag particles captured on an amorphous carbon membrane at the substrate bias of +300 V for (**a**) 1 s; (**b**) 3 s; (**c**) 5 s; (**d**) 7 s; and (**e**) 10 s.

Figure 5 shows the time evolution of TEM images of the sputtered Ag particles captured under the substrate bias of −300 V. Ag particles captured for 1, 3, 5, 7 and 10 s had the average diameters of 1.6 ± 0.12, 1.8 ± 0.24, 2.0 ± 0.14, 2.5 ± 0.09 and 3.0 ± 0.1 nm and the nanoparticle densities of 15,317 ± 454, 21,497 ± 1531, 25,230 ± 1050, 18,415 ± 418 and 17,919 ± 254 per μm^2, respectively. The average size of Ag particles continued to increase with the capture time, but the number density increased up to 5 s then decreased up to 10 s.

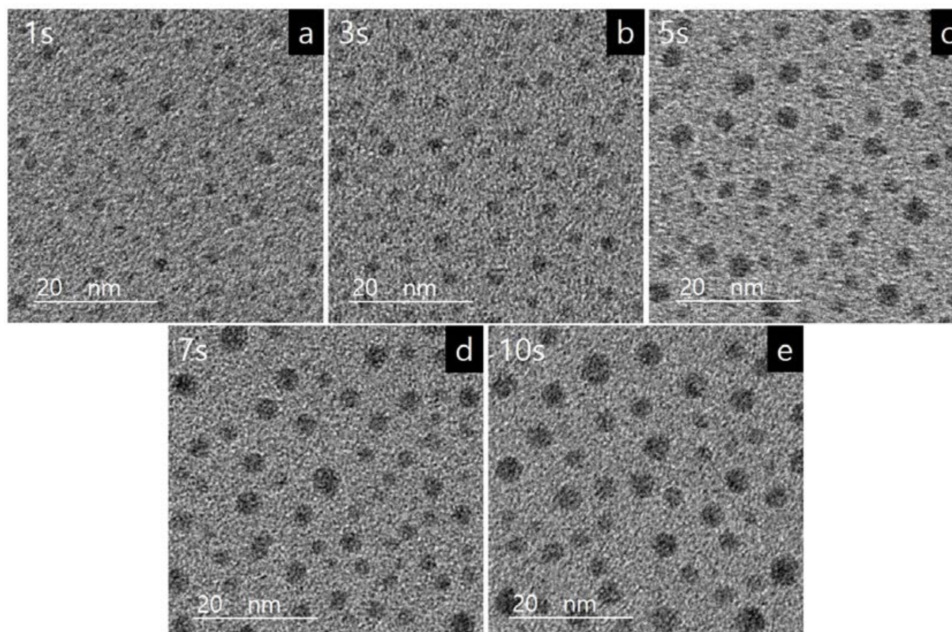

Figure 5. TEM images of Ag particles captured on an amorphous carbon membrane at the substrate bias of −300 V for (**a**) 1 s; (**b**) 3 s; (**c**) 5 s; (**d**) 7 s; and (**e**) 10 s.

In order to compare the time evolution of Ag particles captured up to 10 s under the three bias conditions of 0, +300 and −300 V, their average diameter, number density and total area are plotted against the capture time, respectively, in Figure 6a–c.

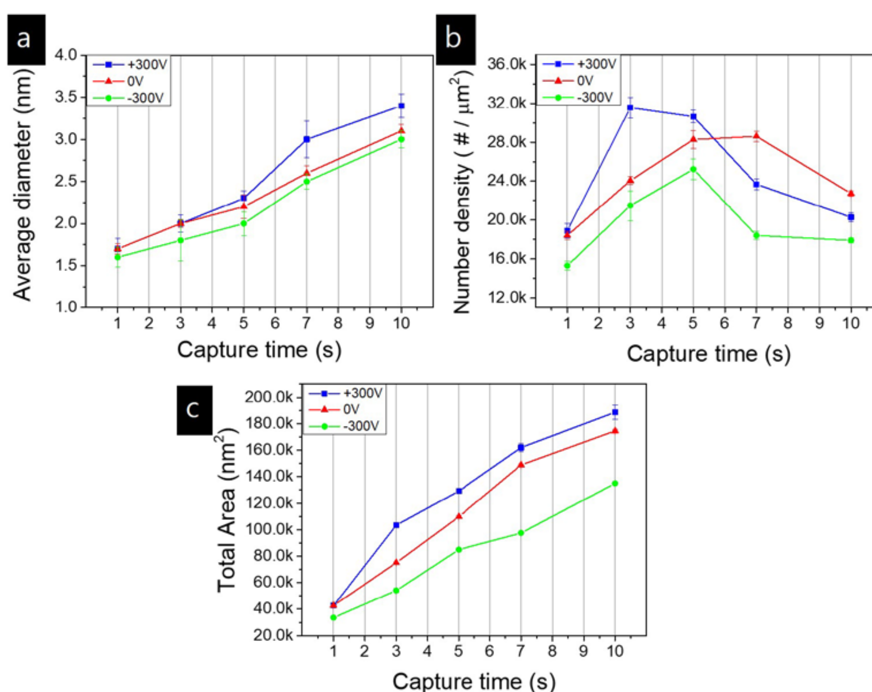

Figure 6. Plots of (**a**) particle average diameter; (**b**) particle count per μm^2; and (**c**) total area of Ag particle per μm^2 against the capture time analyzed by the ImageJ program.

Figure 6a shows that the average diameter of particles captured under +300 V was larger than those captured under 0 and −300 V. Additionally, the size distribution of Ag nanoparticles under each capture condition is shown in Figure S1. Figure 6b shows that the number density of Ag particles increased up to a certain capture time and then decreased in all three bias conditions. Considering the relatively high fraction of the unoccupied area on the carbon membrane shown in Figures 2, 4 and 5, the number density of Ag particles was expected to increase continuously with increasing capture time. This unexpected behavior is discussed later.

Figure 6c shows that the total area of Ag particles on the carbon membrane increased with increasing capture time in all three bias conditions. The total area was largest for +300 V and smallest for −300 V. Since the total area represents the total flux coming from sputtering, it indicates the deposition flux. The difference in the deposition flux under the different bias condition indicates that some of the flux was electrically charged. Considering that the deposition flux became maximum for +300 V, medium for 0 V and minimum for −300 V, an appreciable amount of the flux must have been negatively charged. The positive flux, if any, seemed to be minor or negligible, and the neutral flux seemed to be major. To determine the fraction of the negative flux, the thicknesses of films, which were deposited under the three bias conditions, should be compared. This result will be explained later.

Then, why are small particles in Figures 2a and 3a amorphous? Additionally, why are large particles in Figures 2e and 3b crystalline? When combining the results of Figures 2a,e and 3a,b, it can be said that the Ag particles or films are amorphous in the initial stage of deposition but become crystalline in the later stage. Then, how can such a transition occur at room temperature?

One possible explanation is based on the presence of charge on the growing surface, which is clearly revealed in the current measurement in Figure 1b. According to the phenomenon of melting point depression of small particles [32,33], the melting point of ~1.7 nm Ag particles would decrease far lower than that of the bulk Ag. However, the melting point cannot decrease down to room temperature.

Observing and analyzing the behavior of charged nanoparticles, Hwang [26] suggested a hypothesis that the presence of charge would decrease the bond strength of small nanoparticles and can make them liquid-like.

Based on the hypothesis that small charged nanoparticles have liquid-like behavior, it can be explained why Ag particles of ~1.7 nm in Figures 2a and 3a have an amorphous phase on the amorphous carbon membrane. Considering the appreciable amount of negative current measured during sputtering in Figure 1b, Ag particles of ~1.7 nm in Figures 2a and 3a were expected to be negatively charged. Since negatively charged Ag particles of ~1.7 nm would be liquid-like, they would accommodate the structure of the substrate. If the substrate is crystalline, it tends to have a crystalline structure, and if the substrate is amorphous, it tends to have an amorphous structure. In other words, if charged nanoparticles are small enough to have liquid-like behavior, they tend to have the structural similarity with the substrate to decrease the interfacial free energy. Even if small Ag particles have a crystalline structure in the gas phase, they tend to follow the structure of the substrate. Since the amorphous carbon membrane was used as a substrate for what is shown in Figure 3a, charged Ag particles of ~1.7 nm would have the amorphous structure.

As the size of Ag particles increases, however, the bulk free energy term would become dominant over the interfacial free energy term and then the crystalline phase would become more stable. In this case, the large crystalline Ag particles would remain crystalline even if they landed on the amorphous substrate.

Then, why does the number density decrease with the capture time in Figure 6b? The decrease of the number density occurred in the earliest time of 3 s for Ag particles captured under the bias of +300 V. That leads to another question as to why the bias of +300 V causes the decrease of the number density in the earliest time. These two questions could be approached from the effect of charge.

Considering the negative current data in Figure 1b, an appreciable amount of the negative flux including electrons would exist in the sputtering chamber. The largest total area of Ag particles in Figure 6c for the bias of +300 V indicates that the bias of +300 V attracts the negatively charged flux. As a result, the largest number of negative charges would build up on the Ag particles for the bias of +300 V. The decrease of the number density in Figure 6b indicates that the Ag particles undergo coalescence accompanied by the movement of the center of the particle mass. For such movement, a force between Ag particles should exist. The electrostatic interaction between the charged spherical conducting particles of the same sign can be attractive when their size difference is large enough, considering the following equation [34].

$$F = \frac{q_1 q_2}{4\pi\varepsilon_0 d^2} - \frac{q_2^2 r_1 d}{4\pi\varepsilon_0 (d^2 - r_1^2)^2} - \frac{q_1^2 r_2 d}{4\pi\varepsilon_0 (d^2 - r_2^2)^2} + \ldots, \quad (1)$$

where the sphere of radius r_1 has a net charge q_1 and the other of radius r_2 has charge q_2; d is the distance between the particle centers and $1/4\pi\varepsilon_0$ the permittivity. The first term is the well-known Coulomb equation, which can be attractive or repulsive depending on the signs of the two interacting particles. The second and third terms come from the image force, which are attractive regardless of the sign of the charge. From the fourth term, it is the corresponding to the second image force by the first image force from the second and third terms. Actually, these values are very small and negligible. This equation reveals that if a large spherical particle has a large number of charges, it will attract a small charged particle of the same sign.

The decrease of the number density occurs after 3, 5 and 7 s, respectively, for the biases of +300, −300 and 0 V. Therefore, it seems that the magnitude of the attractive Coulomb interaction between charged Ag particles of the same sign described by Equation (1) would be in the order of +300; −300 and 0 V. We do not clearly understand why the bias of −300 V has a stronger effect than that of 0 V. One possibility could be that the bias of −300 V builds up an appreciable number of positive charges on Ag particles.

3.2. Ag Thin Film Deposition and Analysis

In order to examine the effect of the negatively charged particles on the thin film growth, Ag thin films were deposited for 30 min under the conditions where biases of +300, 0, and −300 V were applied to the substrate holder. Figure 7 shows cross-section FESEM images of the Ag films deposited on a Si substrate. Thicknesses of the Ag thin films, determined by the cross-section FESEM images, were 68.9, 77.6 and 85.0 nm, respectively, for the biases of −300, 0 and +300 V. Compared to the thickness of the film deposited under 0 V, the thickness of the film deposited under +300 V increased by 9.5 % and the thickness under −300 V decreased by 11.2 %. The decrease of the film thickness under −300 V would have come from repelling negatively-charged particles. The increase of the film thickness under +300 V would have come from attracting negatively-charged particles. Such a bias effect on the film thickness indicates that roughly 10% of the flux was negatively charged and the amount of positively charged flux was negligible.

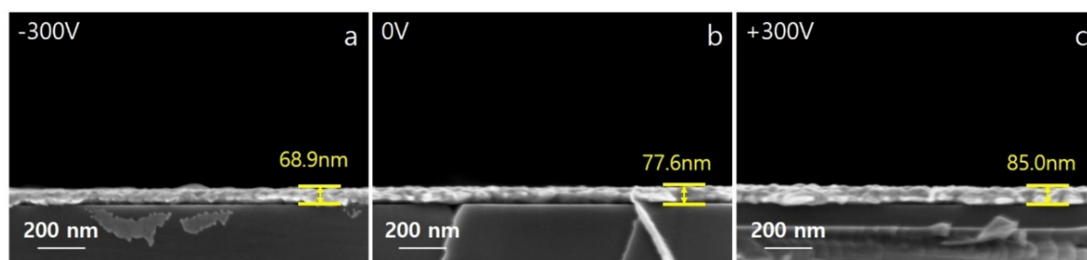

Figure 7. Cross-section FESEM images of the Ag films deposited on Si substrates at the electric biases of (**a**) −300 V; (**b**) 0 V; and (**c**) +300 V.

In order to examine how the deposition of the negatively-charged flux affects the film quality, the surface morphology of films was observed by FESEM and the crystallinity of films was analyzed by XRD. Figure 8 shows top-view FESEM images of Ag films deposited on a Si substrate. The grain size of the thin film deposited under +300 V (Figure 8c,f) was larger than that deposited under 0 V (Figure 8b,e) and that deposited under −300 V (Figure 8a,d). The grain size became larger under the condition of high atomic mobility, which would be favored by the highest charge density condition of Ag particles deposited under the bias of +300 V (Figure 8c,f). The difference in the grain size among Figure 8a–c can also be explained by the charge effect.

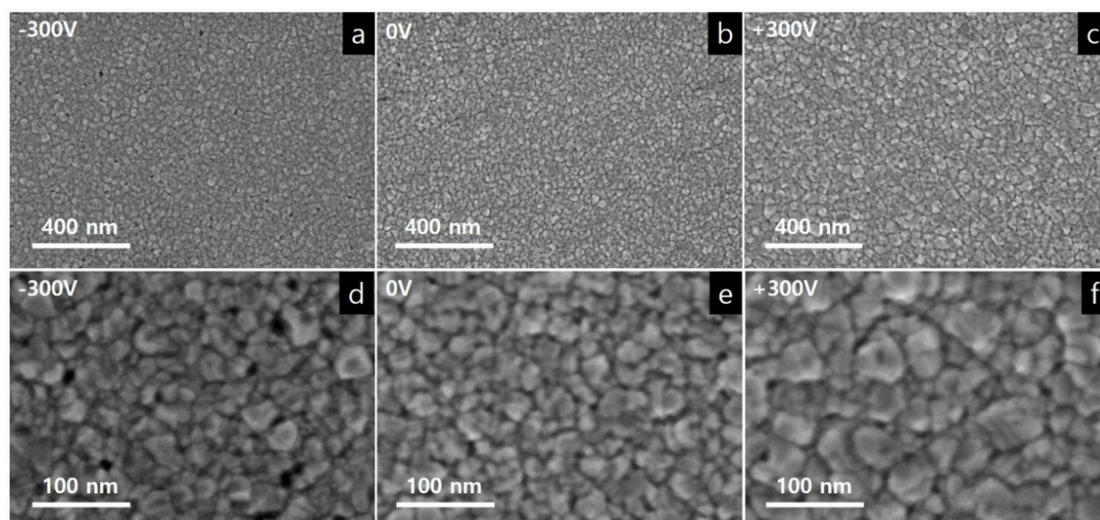

Figure 8. Top-view FESEM images of (**a**–**c**) low magnification and (**d**–**f**) high magnification of the Ag films deposited on Si substrates at the electric biases of (**a**,**d**) −300 V (**b**,**e**) 0 V and (**c**,**f**) +300 V.

Figure 8a,d shows some pores among grains in comparison with Figure 8b,e and Figure 8c,f, where pores were hardly found. Such pore formation in Figure 8a,d seems to be related to the repulsion of negatively-charged Ag particles by the bias of −300 V. Therefore, the pore formation is attributed to the lack of charged Ag particles, which have a liquid-like property or high atomic mobility. The lack of negatively-charged Ag particles might also be related with the small grain size in Figure 8a,d.

The large grain size would result in the high crystallinity. In relation to this, XRD spectra of the films deposited under −300, 0 and +300 V are compared in Figure 9. The peaks at 2θ = 38.11° and 44.27° indicate (111) and (200) orientations of Ag, respectively. When +300 V was applied, both peaks of (111) and (200) showed the highest intensity. On the other hand, when −300 V was applied, both peaks of (111) and (200) showed the lowest intensity. The crystallinity of the Ag thin films can be compared using a full width at half maximum intensity (FWHM) of the (111) peak. The FWHM is inversely proportional to the grain size according to the Scherrer equation,

$$\tau = \frac{K\lambda}{\beta \cos \theta} \tag{2}$$

where τ is the mean size of the grain, K is a dimensionless shape factor, λ is the X-ray wavelength of Cu $K\alpha_1$, β is the FWHM and θ is the Bragg angle, so the smaller the FWHM, the better the crystallinity [35]. The film had the lowest FWHM value of 0.44 when the substrate bias was +300 V, and the highest value of 0.53 when the substrate bias was −300 V. It means that for +300 V, the film had the largest grain, which agrees with the result in Figure 8. Therefore, it can be said that the Ag film of the best crystallinity among the three bias conditions was obtained when +300 V is applied.

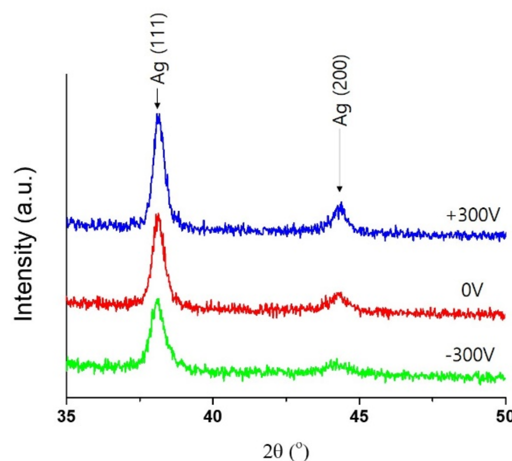

Figure 9. XRD data of the Ag films deposited at the electric biases of −300, 0 and +300 V in the 2θ range of 35–50°. The FWHMs of (111) peaks for −300, 0 and +300 V are 0.53, 0.47 and 0.44, respectively.

The resistivity was measured to evaluate the Ag thin film quality. Figure 10 shows the resistivity of each Ag thin film deposited under each bias condition. The theoretical resistivity of Ag was 1.59 μΩ·cm (at 20 °C). The resistivities of the Ag thin films with +300 and −300 V applied to the substrate holder were, respectively, smallest with 3.67 μΩ·cm and highest with 8.87 μΩ·cm. As in the results of Figures 8 and 9, the Ag thin film with +300 V applied to the substrate showed the best film quality.

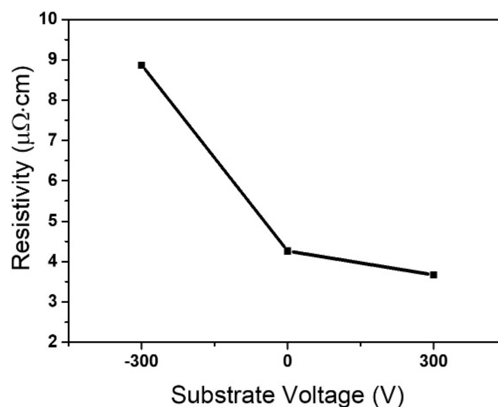

Figure 10. Resistivity of the Ag films deposited at the electric biases of −300, 0 and +300 V.

4. Conclusions

The generation of charged Ag particles and their contributions to film growth were confirmed through the bias experiment and the current measurement during the DC magnetron sputtering. Roughly 10% of sputtered Ag particles were negatively charged and the positive bias applied to the substrate holder increased the film growth rate and produced a film of better crystallinity than that produced by the negative bias. Based on these results, we suggest that the bias can be a new process parameter in sputtering.

Supplementary Materials: The following are available online at http://www.mdpi.com/2079-6412/10/8/736/s1, Figure S1: Gaussian graph for Ag nanoparticles size distribution under each capture condition.

Author Contributions: Conceptualization, G.-S.J. and N.-M.H.; methodology, G.-S.J.; formal analysis, G.-S.J. and D.-Y.K.; investigation, G.-S.J.; data curation, G.-S.J.; writing—original draft preparation, G.-S.J.; writing—review and editing, N.-M.H.; supervision, N.-M.H. All authors have read and agreed to the published version of the manuscript.

Funding: This research was funded by Global Frontier Program through the Global Frontier Hybrid Interface Materials (GFHIM) of the National Research Foundation of Korea (NRF) funded by the Ministry of Science, ICT and Future Planning (MSIT) (number NRF-2013M3A6B1078874) and the National Research Foundation of Korea (NRF) grant funded by the Korea government (MSIT) (number 2020R1A5A6017701) and BK21PLUS SNU Materials Division for Educating Creative Global Leaders (21A20131912052).

Conflicts of Interest: The authors declare no conflict of interest.

References

1. Kato, K.; Omoto, H.; Tomioka, T.; Takamatsu, A. Visible and near infrared light absorbance of Ag thin films deposited on ZnO under layers by magnetron sputtering. *Sol. Energy Mater. Sol. Cells* **2011**, *95*, 2352–2356. [CrossRef]
2. Lee, K.-C.; Lin, S.-J.; Lin, C.-H.; Tsai, C.-S.; Lu, Y.-J. Size effect of Ag nanoparticles on surface plasmon resonance. *Surf. Coat. Technol.* **2008**, *202*, 5339–5342. [CrossRef]
3. Pan, Y.; Fan, Y.; Niu, J. Optical properties of ultra-thin silver films deposited by thermal evaporation and its application in optical filters. *Infrared Phys. Technol.* **2020**, *104*. [CrossRef]
4. Park, H.K.; Yoon, J.K.; Kim, K. Novel fabrication of Ag thin film on glass for efficient surface-enhanced raman scattering. *Langmuir* **2006**, *22*, 1626–1629. [CrossRef] [PubMed]
5. Park, S.H.; Lee, K.S.; Sivasankar Reddy, A. Low emissivity Ag/Ta/glass multilayer thin films deposited by sputtering. *J. Appl. Phys.* **2011**, *110*, 063508. [CrossRef]
6. Bittner, A.; Seidel, H.; Schmid, U. Electromigration resistance and long term stability of textured silver thin films on LTCC. *Microelectron. Eng.* **2011**, *88*, 127–130. [CrossRef]
7. Tsuda, Y.; Omoto, H.; Tanaka, K.; Ohsaki, H. The underlayer effects on the electrical resistivity of Ag thin film. *Thin Solid Film.* **2006**, *502*, 223–227. [CrossRef]
8. Guzman, M.; Dille, J.; Godet, S. Synthesis and antibacterial activity of silver nanoparticles against gram-positive and gram-negative bacteria. *Nanomedicine* **2012**, *8*, 37–45. [CrossRef]

9. Kim, J.S.; Kuk, E.; Yu, K.N.; Kim, J.H.; Park, S.J.; Lee, H.J.; Kim, S.H.; Park, Y.K.; Park, Y.H.; Hwang, C.Y.; et al. Antimicrobial effects of silver nanoparticles. *Nanomedicine* **2007**, *3*, 95–101. [CrossRef]
10. Shahverdi, A.R.; Fakhimi, A.; Shahverdi, H.R.; Minaian, S. Synthesis and effect of silver nanoparticles on the antibacterial activity of different antibiotics against Staphylococcus aureus and Escherichia coli. *Nanomedicine* **2007**, *3*, 168–171. [CrossRef]
11. Jeon, I.-D.; Kim, D.-Y.; Hwang, N.-M. Spontaneous generation of charged atoms or clusters during thermal evaporation of silver. *Z. Für. Met.* **2005**, *96*, 186–190. [CrossRef]
12. Hajakbari, F.; Ensandoust, M. Study of thermal annealing effect on the properties of silver thin films prepared by dc magnetron sputtering. *Acta Phys. Pol. A* **2016**, *129*, 680–682. [CrossRef]
13. Jung, Y.S. Study on texture evolution and properties of silver thin films prepared by sputtering deposition. *Appl. Surf. Sci.* **2004**, *221*, 281–287. [CrossRef]
14. Maréchal, N.; Quesnel, E.; Pauleau, Y. Silver thin films deposited by magnetron sputtering. *Thin Solid Film.* **1994**, *241*, 34–38. [CrossRef]
15. Xiong, Y.; Wu, H.; Guo, Y.; Sun, Y.; Yang, D.; Da, D. Preparation and characterization of nanostructured silver thin films deposited by radio frequency magnetron sputtering. *Thin Solid Film.* **2000**, *375*, 300–303. [CrossRef]
16. Xu, K.; Hao, L.; Du, M.; Mi, J.; Yu, Q.; Li, S.; Wang, J.; Li, S. Thermal emittance of Ag films deposited by magnetron sputtering. *Vacuum* **2020**, *174*. [CrossRef]
17. Baghriche, O.; Zertal, A.; Ehiasarian, A.P.; Sanjines, R.; Pulgarin, C.; Kusiak-Nejman, E.; Morawski, A.W.; Kiwi, J. Advantages of highly ionized pulse plasma magnetron sputtering (HIPIMS) of silver for improved E. coli inactivation. *Thin Solid Film.* **2012**, *520*, 3567–3573. [CrossRef]
18. West, G.T.; Kelly, P.J.; Bradley, J.W. A Comparison of thin silver films grown onto zinc oxide via conventional magnetron sputtering and hipims deposition. *IEEE Trans. Plasma Sci.* **2010**, *38*, 3057–3061. [CrossRef]
19. Markov, I.V. *Crystal Growth for Beginners: Fundamentals of Nucleation, Crystal Growth and Epitaxy*, 2nd ed.; World Scientific: Singapore, 2003; pp. 1–546. [CrossRef]
20. Taden, A.; Landfester, K.; Antonietti, M. Crystallization of dyes by directed aggregation of colloidal intermediates: A model case. *Langmuir* **2004**, *20*, 957–961. [CrossRef]
21. Gebauer, D.; Völkel, A.; Cölfen, H. Stable prenucleation calcium carbonate clusters. *Science* **2008**, *322*, 1819. [CrossRef]
22. Amos, F.F.; Dai, L.; Kumar, R.; Khan, S.R.; Gower, L.B. Mechanism of formation of concentrically laminated spherules: Implication to Randall's plaque and stone formation. *Urol. Res.* **2009**, *37*, 11–17. [CrossRef]
23. Jung, J.-S.; Lee, S.-H.; Kim, D.-S.; Kim, K.-S.; Park, S.-W.; Hwang, N.-M. Non-classical crystallization of silicon thin films during hot wire chemical vapor deposition. *J. Cryst. Growth* **2017**, *458*, 8–15. [CrossRef]
24. Sadri, B.; Pernitsky, D.; Sadrzadeh, M. Aggregation and deposition of colloidal particles: Effect of surface properties of collector beads. *Colloids Surf. A Physicochem. Eng. Asp.* **2017**, *530*, 46–52. [CrossRef]
25. Song, R.; Krasia-Christoforou, T.; Debus, C.; Cölfen, H. Structure and magnetic property control of copper hydroxide acetate by non-classical crystallization. *Small* **2017**, *13*, 1602702. [CrossRef] [PubMed]
26. Hwang, N.M. *Non-Classical Crystallization of Thin Films and Nanostructures in CVD and PVD Processes*; Springer: Berlin, Germany, 2016; Volume 60, pp. 1–332. [CrossRef]
27. Park, S.-W.; Jung, J.-S.; Kim, K.-S.; Kim, K.-H.; Hwang, N.-M. Effect of bias applied to the substrate on the low temperature growth of silicon epitaxial films during RF-PECVD. *Cryst. Growth Des.* **2018**, *18*, 5816–5823. [CrossRef]
28. Clare, B.W.; Talukder, G.; Jennings, P.J.; Cornish, J.C.L.; Hefter, G.T. Effect of charge on bond strength in hydrogenated amorphous silicon. *J. Comput. Chem.* **1994**, *15*, 644–652. [CrossRef]
29. Kwon, J.-H.; Kim, D.-Y.; Hwang, N.-M. Generation of charged Ti nanoparticles and their deposition behavior with a substrate bias during RF magnetron sputtering. *Coatings* **2020**, *10*, 443. [CrossRef]
30. Chapman, B. *Glow Discharge Processes: Sputtering and Plasma Etching*; Wiley: Hoboken, NJ, USA, 1980; pp. 1–406.
31. Igathinathane, C.; Pordesimo, L.O.; Columbus, E.P.; Batchelor, W.D.; Methuku, S.R. Shape identification and particles size distribution from basic shape parameters using ImageJ. *Comput. Electron. Agric.* **2008**, *63*, 168–182. [CrossRef]
32. Iijima, S.; Ichihashi, T. Structural instability of ultrafine particles of metals. *Phys. Rev. Lett.* **1986**, *56*, 616–619. [CrossRef]

33. Zhang, M.; Efremov, M.Y.; Schiettekatte, F.; Olson, E.A.; Kwan, A.T.; Lai, S.L.; Wisleder, T.; Greene, J.E.; Allen, L.H. Size-dependent melting point depression of nanostructures: Nanocalorimetric measurements. *Phys. Rev. B* **2000**, *62*, 10548–10557. [CrossRef]
34. Dove, D.B. Possible influence of electric charge effects on the initial growth processes occurring during the vapor deposition of metal films onto substrates inside the electron microscope. *J. Appl. Phys.* **1964**, *35*, 2785–2786. [CrossRef]
35. Muniz, F.T.; Miranda, M.A.; Morilla Dos Santos, C.; Sasaki, J.M. The scherrer equation and the dynamical theory of X-ray diffraction. *Acta Crystallogr. Sect. Afound. Adv.* **2016**, *72*, 385–390. [CrossRef] [PubMed]

© 2020 by the authors. Licensee MDPI, Basel, Switzerland. This article is an open access article distributed under the terms and conditions of the Creative Commons Attribution (CC BY) license (http://creativecommons.org/licenses/by/4.0/).